iJRASET
International Journal For Research in Applied Science and Engineering Technology

INTERNATIONAL JOURNAL FOR RESEARCH

IN APPLIED SCIENCE & ENGINEERING TECHNOLOGY

Volume: 10 **Issue:** VIII **Month of publication:** August 2022

DOI: https://doi.org/10.22214/ijraset.2022.46195

www.ijraset.com

Call: 08813907089 | E-mail ID: ijraset@gmail.com

International Journal for Research in Applied Science & Engineering Technology (IJRASET)
ISSN: 2321-9653; IC Value: 45.98; SJ Impact Factor: 7.538
Volume 10 Issue VIII August 2022- Available at www.ijraset.com

Preparation Properties and Device Application of β- Ga_2O_3: A Review

Ashwani Kumar[1], Sheetal Singh[2], Divyanshu Shukla[3]
[1, 2]*Electronics and Communication Engineering Department,* [3]*Mechanical Engineering Department, Institute of Engineering and Technology (IET), Lucknow, India 226021*

Abstract: ***Extremely wide-bandgap β-Ga_2O_3 is a new way semiconducting has wide range of application such as electronics devices operated at high temperature and short-wavelength optoelectronics. It has a wide bandgap of 4.5eV -4.9 electron volt (ev) and great thermal stabilization up to 1400^{0}C, opening new possibilities for various device applications. The development of β-Ga_2O_3 thin film growth, characteristics, and device demonstrations is reviewed in this study. The methods used to demonstrate great-quality β-Ga_2O_3 thin film growth with controlled doping are discussed. Monoclinic β-Ga_2O_3 applications in devices are also discussed. Finally, a conclusion will be offered and future research perspectives on this key semiconducting material.***
Keywords: Ga_2O_3, optoelectronic devices, Stucture of Ga_2O_3, Photodetector,

I. INTRODUCTION

Ultrawide bandgap (UWBG) semiconductor material (Ga_2O_3) coming out as a new generation power devices operating at high voltages in electronics and deep ultraviolet (DUV) star blind photodetectors contribute to its distinctive material characteristics. There are various polymorphs which are named as (α, β, γ, δ and ε), β-Ga_2O_3 with a monoclinic crystal structure represents the foremost thermally stable material. β-Ga_2O_3 contains a temperature bandgap ~4.5-4.9 eV. It additionally has wonderful chemical, mechanical- strength and thermal-stability at elevated temperatures variation . because of its ultrawide bandgap that similarize to the cut-off wavelength equivalent to 250 nm, β-Ga_2O_3 is solar-blind. As a result, DUV photodetectors supported not need any supplementary filter. It additionally avoids alloying and therefore simplifies the fabric growth method. Moreover, β-Ga_2O_3 primarily based on field result transistors, diodes will have great device properties which includes large breakdown voltage aalongwith high power and low loss because of its terribly massive bandgap. Coordinative relationship exhibit between the bandgap Eg and breakdown electrical fields ,the Ebr of β-Ga_2O_3 is predicted to be worth 6-8 MV/cm [1]. Higher value of Ebr is fascinating property of β-Ga_2O_3 as a result of the Baliga's figure-of-merit (FOM), parameter to judge however appropriate a cloth is for power devices, diect effect to Ebr however, is merely linearly variation to quality. As compared to a GaN, the conductivity loss of β-Ga_2O_3 power devices may be similar to one order of magnitude lower at constant breakdown voltage. a lot of well, top-quality top quality can be synthesized in massive volumes by climbable and low-price melt-growth techniques. This addresses these industrial constraints of attack and GaN primarily based device technologies that lack reasonable native substrates. Scientific studies and analysis in β-Ga_2O_3 has greatly point of interaction recently.

II. FEAUTURES OF β-Ga_2O_3

A. *Structure Of B-Ga_2o_3*

Among all different structure of metallic element compounds, This material has involved the attraction due to handiness and speculative properties. At a given temperature, it is stable and variation takes place until melting point. β-Ga_2O_3 exhibit a C-centered monoclinic building block with C2/m space . It holds some crystallographically idistinguishable one Gallium positions, one of the atom is tetrahedral (I) and the another octahedral Gallium (II). O_2 have some crystallographically various dimension and area units depicted as O (1^{st}), O (2^{nd}) and O (3^{rd}), severally. Area of $2O_2$ unit synchronal trigonally and another is synchronized tetrahedrally.
Ga_2O_3 is a TCO that can take on a variety of polymorphs, including and [2], which act as conductor or insulators reliant upon the improved circumstances used. Distinctive band alignments can be found in each polymorph [3]. Furthermore, in the crystal lattice, all polymorphic have somewhat different material properties. Polymorphs differ from each other in a variety of ways. Including characteristics of the crystal space and the quantity of Ga^{3+}. In coordination Under certain conditions, each polymorph displays its Ga_2O_3 phases. Under specific circumstances [4]. The the phases are defective spinel (γ-Ga_2O_3), rhombohedral (α-Ga_2O_3), cubic (δ-Ga_2O_3), monoclinic (β-Ga_2O_3), , and orthorhombic of (Ɛ-Ga_2O_3) crystal structure are among the polymorphs of Ga_2O_3 [5].

ISSN: 2321-9653; IC Value: 45.98; SJ Impact Factor: 7.538
Volume 10 Issue VIII August 2022- Available at www.ijraset.com

Figure 1 depicts well-known polymorph crystal formations. These polymorphs, which are members of the Ga_2O_3 family, have distinct structures.

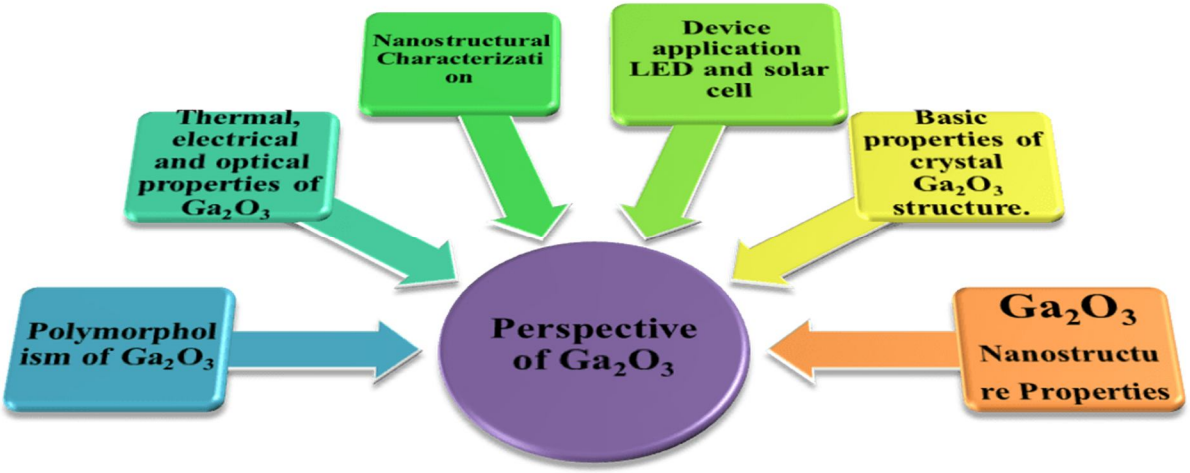

Figure 1 Properties of Ga_2O_3.

Among all Ga_2O_3, β-Ga_2O_3 is largect stable at polymorphic phase. The interconversion connection between Ga_2O_3 and other elements is depicted in polymorphs. α-Ga_2O_3 can be transformed into β-Ga_2O_3 by heating it to above 600^0C. Meanwhile, only γ-Ga_2O_3 and δ- Ga_2O_3 are possible. Under dry conditions, they were heated to temperatures of 650°C and 870°cconsecutively, to transform them into the β-Ga_2O_3 phase. In contrast, δ-Ga_2O_3 can only be converted to β-Ga_2O_3 when heated to 300°C in a moist environment as described in Figure 2.

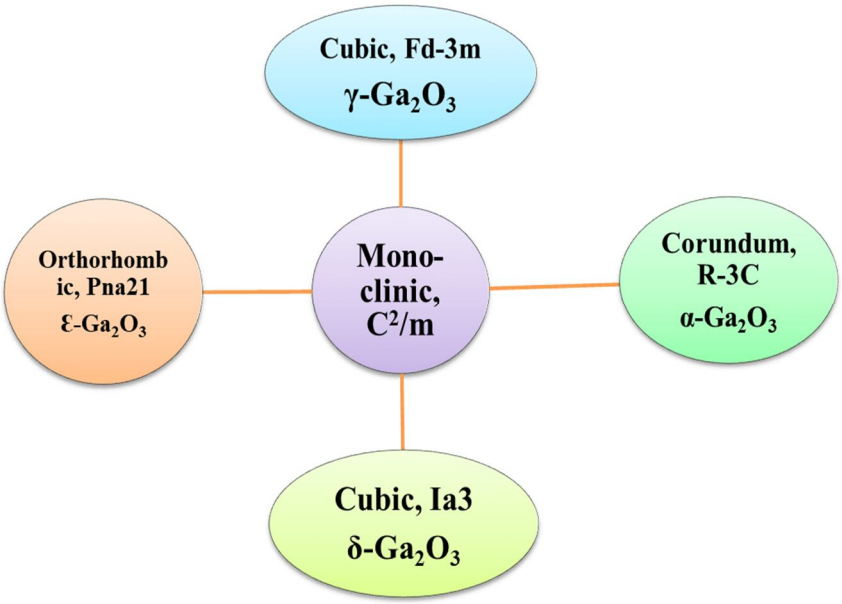

Figure 2 Interconversion of various phase of Ga_2O_3.

The highest electrical field for breakdown region is related to them. The strength of reverse break down field is commonly used in FOMs, with scales which are expressed as the bandgap typically in the 2–2.5 range. The product of power frequency for RF amplification is known as Johnson's FOM (JFOM). A high current density is produced by a high electron saturation velocity. Ga_2O_3 broad bandgap allows it to operate in high temperatures conditions, and its large critical field allows it to operate in high voltages.
***Table** 1* provides a detailed comparative analysis of Ga_2O_3 with other wide bandgap semiconductors (WBS). Ga_2O_3 has a high FOM for low power at high-frequency devices switching operated in the frequency range of GHz, as seen in this table. When compared to Ga_2O_3, the over cost of GaN substrates may limit their large term viability. Different semiconductors' suitability.

Table 1 Material comparison of different parameters-

Material parameters	Si	β-Ga_2O_3	Diamond	GaN	GaAs	Unit
Electron mobility	1480	300	2000	1250	8480	(cm^2 /Vs)
Saturation velocity	1	2	1	2.5	1.2	(10^7 cm/s)
Baliga higher frequency	1	142.2	1501	100.8	10.1	-
Dielectric constant	11.1	10	5.5	3.4	1.43	-
Thermal conductivity	1.5	0.3	20	2.3	0.5	(W/cm K)
Bandgap	1.1	4.85	5.5	3.4	1.43	(AW^{-1})
Breakdown field	0.3	8	10	3.3	0.4	-

B. Thermal Characteristics Of B-Ga_2o_3

β-Ga_2O_3 has minimum thermal conductivities in comparison to alternative semiconductors like set on, sapphire and GaN. Its thermal physical phenomenon is half of magnitude and sapphire of order one smaller than GaN [6]. The thermal physical phenomenon in β-Ga_2O_3 is enthusiastic about its lattice direction owing to its crystalline property. it had been depicted that the best physical phenomenon at 010 diretion having the value 27 W/m-k in comparison to 100 direction lowest thermal phenomenon have 10.9 W/m-k [7,8].

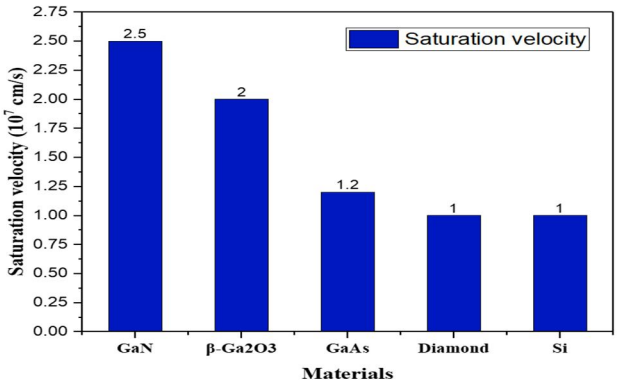

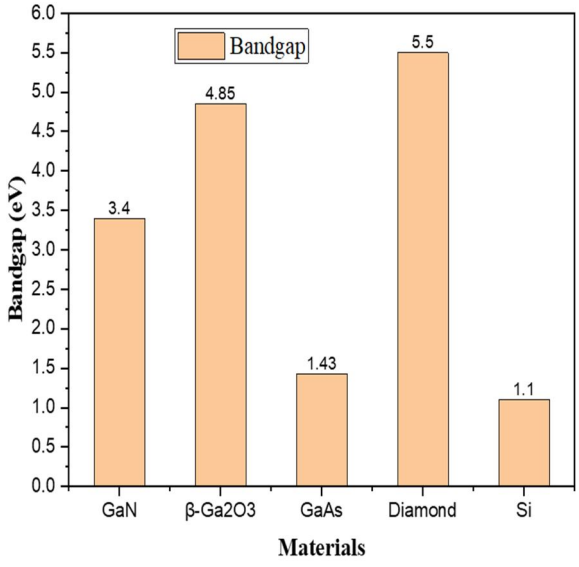

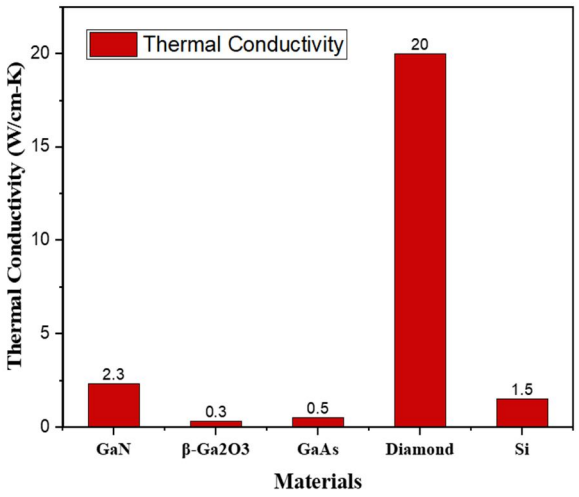

Figure 3 Analsis graph of different parameters on different materials.

III. GROWTH OF β-Ga_2O_3

A. *Production Of B-Ga_2o_3 By Bulk Growth Method*

Depending on device application of β-Ga_2O_3 there are various structural standards, doping of rare earth material exhibits.β-Ga_2O_3 substrates has glorious structural coordination and manageable doping areas unit crucial for realizing applied device applications. Production of good quality crystals of substrates is produced by EFG. floating zone [9,10] and Czochralski [11,12] ways. The production of substrat made by this method is scalable and low price [13]. β-Ga_2O_3 substrates show an n-type physical phenomenon that is meant to be owed to the Si impurity icluded Ga_2O_3 powder supply. Fe, Mg used as doping element for the production of semi insulationg gallium oxide substrates [14,15].

B. *β-Ga_2O_3 Thin Film Growth Method*

β-Ga_2O_3 skinny Film Growth have fully grown by numerous ways together with MBE [9,16], MOVPE) [17], HVPE [18], and LPCVD [19].

C. *β-Ga_2O_3 MBE Growth Method*

MBE is a method to decrease impurity level and produced good quality skinny films. It grows skinny films with low impurity levels to an ultrahigh atmosphere having vaccume and high purity. Production of β-Ga_2O_3 by MBE growth process is taken place by temperature changes in range 500^0C to 800^0C. For O supply, each O_2 [20], [21][22] and O_3 [23] area unit getting used. the expansion rates of MBE mature skinny films vary between 50 -180 nm/hr. The restricted rate of growth is thanks to growth dynamics related to the technique. Sources Sn/ Ge used as the doping material in the production of β-Ga_2O_3 by the process moleculaer MBE. [23], [24]. The use of Sn as acareer concentration varies in range of 10^{16} to 10^{19} [23]; whereas the carrier concentration has vary between 10^{18}-10^{19} cm^{-3} exploitation Ge [24]. the most realizable quality up to now exploitation tin and Ge were ~150 cm^2/Vs and 97 cm^2/Vs, consecutively.

D. *β-Ga_2O_3 MOVPE Growth*

MOVPE business technique for manufacturing prime quality III-V nitride growing. Production higher volume material is produced by deposition process. MOVPE growth in β-Ga_2O_3 skinny films completing within the temperature varies between 550 ^{o}C-850 ^{o}C TMGa, TEGa, and high purity oxygen are used as sources. the expansion rates of the MOVPE mature skinny films vary within vary in range of 120 -750 nm. N-type doping of β-Ga_2O_3 films grown by MOVPE each doping material of Sn and Si were used [25], [26]. Therefore, laborious to grow skinny film have lesser doping concentration when higher dopant flow increment. In additionally procedures totally different defects within the skinny films that in turn lowers the fabric quality. Just in the case of Si, it forms SiO_2 thanks to the sturdy affinity of Si to O. Resulted, Si dopants aren't electrically active. the best-declared quality up to now was 130 cm^2/Vs for Si-doped skinny films have the concentration of ~1x10^{17} cm^{-3} [25].

E. β-Ga_2O_3 HVPE Growth

HVPE is low cost-effective technique given by Japan which will manufacture the materials by the help of sensible crystalline quality and a quicker rate of increment. HVPE growth of β-Ga_2O_3 films are done at ~1050^{o}C exploitation of metal chloride and oxygen as a precursors. Nitrogen is introduce as a carrier Gas. The fastest rate of growth reportable to this point is ~25 μm/hour ,when homoepitaxial layer of β-Ga_2O_3 oriented at (001) direction substrates [27].Semiconductor compound Sicl4 used as economical dopant when N-type HVPE increment skinny film are produced. Thanks to the quick rate of growth, skinny films suffer from surface roughness. As result, an additional sprucing procedure is needed previous device process. Additionally, thanks to the use of GaCl as Ga supply, the skinny films show the prevalence of Cl impurity and defect.

F. β-Ga_2O_3 LPCVD Growth

It is a cheap technique that offers top-quality material with a quick rate, controlled doping and high quality [28]. β-Ga_2O_3 films are produced when temperature changes from 780^{0}C- 950^{0}C by LPCVD increment. It uses high purity gold Ga and O_2 gas because of the source. $SiCl_4$ shows N-type dopant behavior.

In range growth of β-Ga_2O_3 skinny films varied between 0.5-10μm/h has been achieved through the LPCVD growth technique by dynamic the expansion parameters like growth temperature, pressure and precursor rate. *Figure 4* shows the highest read FESEM image for heteroepitaxial accidentally doped (UID) β-Ga_2O_3 skinny film produced for 2h on the c-plane sapphire at 800^{o}C. the skinny film consists of tiny domains that have pseudo polygonal shape morphology. The skinny film exhibits a thickness of 3.42μm. and provides a rate of 1.7μm/h for this film. the complete breadth at 0.5 most (FWHM) of the curve is presented as 1.494^0. temperature absorber spectrum is a basic parameter for understanding optical features of β-Ga_2O_3 . Figure 4 shows peak absorption annum at 260nm which lies in deap ultraviolet radiation and production of gallium oxide film at 900^{0}C. The skinny film incorporates a sturdy absorption within the deep ultraviolet radiation region absorption edge at around 260 nm.

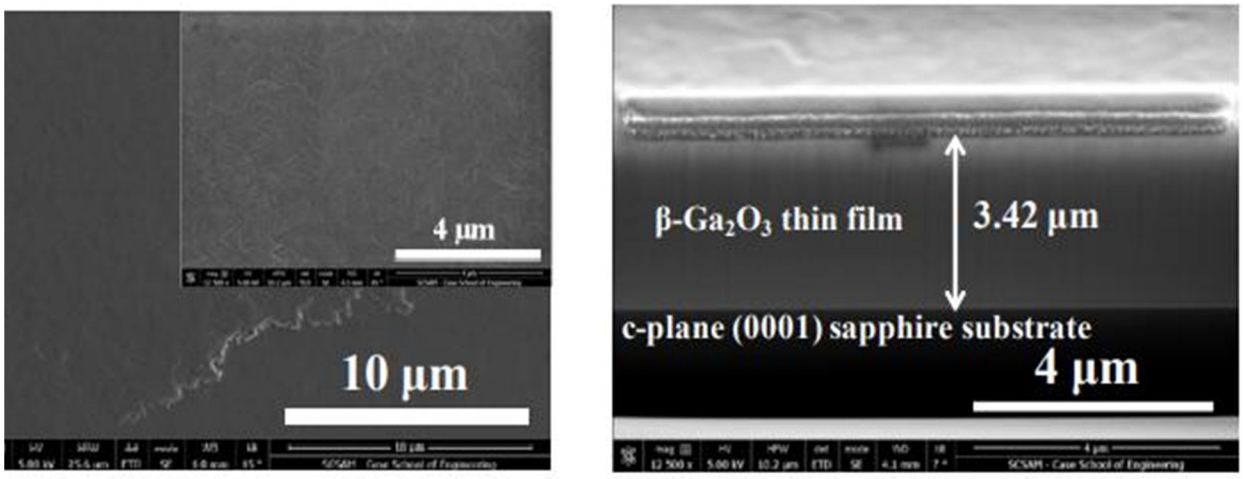

Figure 4 Top view and Cross-sectional FESEM presentation of β-Ga_2O_3. [29] .

Electrical LPCVD grown method used for hetroepitaxial βGa_2O_3 is best method to show electrical characterstics. The amount of carrier varies from 10^{16} to 10^{19} cm^{-3} with the help of change in doping supply rate. Value of measured space temperature Hall quality ranged between 8- 42.35 cm^2/volt sec. With any optimization of the growth condition, the lepton Hall quality will reach >100 cm^2/Vs with a doping concentration within the low-10^{18} cm^{-3}. By standardization of the expansion conditions, a similar rate for the homoepitaxial skinny films will be achieved. because of the heteroepitaxial ones. FESEM image of TEM ready by FIB from a homoepitaxial β-Ga_2O_3 skinny film. The crystal quality of the homoepitaxial skinny film was familiarised by an XRD curve. the XRD curves of (-42-2) reflection of the β-Ga_2O_3 homoepitaxial layer processed at temperatures of 900^{o}C and 950^{o}C. The XRD rocking curve full breadth at 0.5 most (FWHM) of (-42-2) peak for the layer fully grown at 900^{o}C and therefore the substrate was 40 and 20 arcsec, severally..

Note that there no evidencesthus far on achieving semiconductive Ga_2O_3 material with p-type dopant because of the expected giant ionization energies, presence ofnative defects (1).. The understanding of defects has been for the most part driven by initial principal calculations exploitation of totally different approaches [30].

ISSN: 2321-9653; IC Value: 45.98; SJ Impact Factor: 7.538
Volume 10 Issue VIII August 2022- Available at www.ijraset.com

IV. β-Ga_2O_3 DEVICES

A. *Making Of B-Ga_2o_3*

Etching required for intra-device in order to expose layers for successful contact. Studies should be carried out to fully understand the wet and dry etching of β-Ga_2O_3, as well as the associated process and effects the material characteristics. Any device that wants to deliver low contact resistance at moderate hardening temperatures needs high-quality contacts. Several I-V for based devices have been discovered to be only quasi-linear low current, highlighting the requirement of improved β-Ga_2O_3 contact techniques for many mature semiconductors..

Any semiconductor material gate insulator must meet three requirements:it must be thermodynamically stable with the semiconductor and not react during processing, it must have a high-quality interface with low defect and entice density,it must have sufficient band offsets to act as each lepton and hole barrier. The device's performance is mostly determined by the band offsets and kind of band alignment. The ultra-wide bandgap of -Ga2O3 restricts gate dielectric market decisions to those having bandgaps more than 6 eV, such as SiO2, Al2O3, HfO2, ZrO2, and LaAlO3.. The use of β-Ga_2O_3 to measure band offsets of various dielectrics is still in its early stages. Additional print conditions optimization for patterning the dielectrics and improving their interface quality with β-Ga_2O_3 is still required..

β-Ga_2O_3 based power devices may require thermal control due to the fabric's limited and anisotropic thermal conduction. This problem can be solved by using heat sinks such as diamonds or transferring to a metal substrate.. direction presently being developed for GaN power physics. because β-Ga_2O_3 has a lower thermal conductivity than other wide bandgap materials, these techniques should be highly feasible for using β-Ga_2O_3 in high power devices.

B. *β-Ga_2O_3 Field Impact Transistors*

Field impact transistors (FETs) based on Ga_2O_3 have lately been explored due to its potential applications as next-generation physics.. FETs with a single Ga_2O_3 grown by MBE and MOVPE are indisputable. [31]. According to numerous teams, FETs based on slender flakes and nanomembranes exfoliated automatically from Ga_2O_3 single structure have also been developed. [32].

C. *β-Ga_2O_3 Schottky Barrier Diodes*

Because of the expected strong breakdown field of force (Eb 6-8 MV/cm) and low electron quality (200-300 cm2/Vs), β-Ga_2O_3 is expected to have a much higher Baliga's figure of merit (FOM) (Eb3, where is the relative insulator constant) than assault or GaN. β-Ga_2O_3 is based mostly on Schottky barrier diodes (SBDs), which have indisputable device properties. [33]. The best breakdown voltage so far produced by HVPE for β-Ga_2O_3 drift layer-based largely field-plated (FP) SBD adult is 1076 V. [34].

D. *β-Ga_2O_3 Photodetectors*

Deep-ultraviolet (DUV) solar-blinds with a cutoff 280 nm wavelength photodetectors (PDs) have gotten a lot of attention because of their capabilities in missile tracking, flame detection, and chemical/organic analysis, among other things.. Due to its perfect structure, a bandgap equivalent to 4.5-4.9 eV, and excellent chemical, mechanical, and thermal stability, monoclinic β-Ga_2O_3 is a good option for DUV PD.. As a result, in recent years, significant research on β-Ga_2O_3 has focused on completely solar-blind PDs. The active layers for PDs were β-Ga_2O_3 nanomaterials [36], thin films [37], and single crystals [38].. However, results of interband illness stages at the PD tool overall performance are nevertheless now no longer properly understood yet.

E. *Ga_2O_3 Gas Sensors*

Ga_2O_3 primarily based on thin films havestudied recently [35].Sensors related to oxygen feature primarily based totally on the truth that the conductivity of β-Ga_2O_3 skinny movies is inversely relation to the oxygen pressure withinside the surrounding . temperatures around 600^0C, the oxygen sensitivity of Ga_2O_3 reduces considerably and it is able to rather be used to discover lowering gases such as hydrogen.

The H_2 brought about modifications withinside the electrical conductivity of Ga_2O_3 end result from the hydrogen at the complete process of the Ga_2O_3 with the next electron switch from the adsorbed hydrogen into Ga_2O_3.

However, it needs to be talked about that the reaction of the Ga_2O_3 sensor in the direction of lowering additives like ethanol can not be overlooked in contrast with oxygen reaction even at the excessive temperature of 800 ^oC The cross-sensitivity to lowering additives can be decreased with the aid of using extra catalytic or clear out.

V. Ga_2O_3 PHOTOCATALYSIS

Photocatalytic structures the use of sun strength have attracted an awful lot of interest because of their ability the comfort the environmental difficulties. Ga_2O_3 is the most intriguing photocatalyst substances since it has demonstrated excellent photocatalytic properties for a variety of processes, including water splitting, carbon dioxide reduction, and methane conversion [40], as well as the degradation of natural compounds.. The specific structures coordinatively unsaturated Ga^{3+} cations, which are regarded to be crucial for hydrocarbon activation in the CO_2 environment, are credited with Ga_2O_3 catalytic activity.

VI. III-NITRIDES of β-Ga_2O_3 EPITAXY

Regardless of the current advancement in bulk GaN unmarried crystal fabrication methods, GaN substrates are expensive and difficult . As a result, the majority GaN devices are made using heteroepitaxial of substrate such as sapphire, silicon.However, there are still challenging conditions with those substances, such as sapphire's insulating ability, which makes it impossible to produce vertical gadgets. In the case of SiC, extremely expensive and has a lot of optical absorption in the blue part of the spectrum. A significant thermalmismatch, chemical interaction with GaN within the expanded surroundings, and opaqueness in visible and UV spectrum are all concerns associated with silicon. Monoclinicβ- Ga_2O_3 is an excellent choice for serving as an enhanced substrate for III-nitrides because it combines the visible and conductive substrate. Excessive high-satisfactory bulk β- Ga_2O_3 crystals can be created more advantageously by melt-increase procedures such as Czochralski and EFG at a cheap value and high throughput.. As a result, various reviews on the synthesis of GaN epilayers on different orientations of β-Ga2O3 substrates using MOVPE, MBE [41], and HVPE have been published recently.

VII. OPTICAL CHARACTERISTICS OF Ga_2O_3

At a wavelength of 250 nm, Ga_2O_3 is visible optically. Ga_2O_3 has a large bandgap, which is most noticeable in the UV–visible range of spectrum. The color of the crystal might be affected by impurities, flaws, or varied specific boom circumstances [36]. The conductivity and optical residences of the mild spectrum have a substantial link in this state of affairs. Because of a few modest absorptions within the blue observed mild variation spectrum, insulated β-Ga_2O_3 crystals are either have no color or have a mild yellowish tint.

The optical transmittance spectra of Ga_2O_3 are considerably affected by different concentrations of free electrons [37]. Ga_2O_3 was discovered in the DUV spectral band at first. Transmittance spectra for crystals with no regard for electrons have absorption range in between 255–260 nm. With the help of improved the electron attention have origin from various contaminants, the absorption range have shifts toward the NIR(Non Infra red) wavelength region area with total transparency. The absorption spectrum is responsible for the transition from the VB (valence band) into conduction band, showing that the transmittance spectrum is between 255nm and 260nm. within the visible and NIR(Non infra red) wavelengths degenerate with affluence in loose electrons attention. On the wavelength area between 255 and 260 nm, a rapid cutoff absorption facet was detected [38].

The effect of optical transition strength on annealing temperature was previously demonstrated [39]. An change in bandgap ranges from 4.82 eV to 4.86 eV is caused by an excessive annealing temperature. UV–Vis-NIR(ultra violet-visible-infrared region) and photoluminescence (PL) spectroscopy are the optical characterization methodologies used. Changing the bandgap strength or optical residences is especially possible when employing different annealing temperatures. This location is particularly useful for evaluating Ga_2O_3 software in optoelectronic devices.

β-Ga_2O_3 emits three bands of light: UV (3.2–3.6 eV), inexperienced region (2.4 eV)and blue region (2.8–3.0 eV) [40]. The pattern practice technique and contaminants appear to have little effect on UV band emission. UV light coming from band facet recombination is implausible, as evidenced by the β-Ga_2O_3 bandgap of 4.8 eV. When loose electrons and self-trapped holes recombine, β-Ga_2O_3 will only appear in UV band. In β-Ga_2O_3 crystals, where Oxygen (O) vacancies are relates conductivity properties involved blue emission, A link between blue band depth and resistivity [41].

The recombination of electrons and holes by Hartwig and Kellendonk [42] allowed β-Ga_2O_3 to produce a blue moderate spectrum. However, the following doping with exact factors such as Be, Li, Fe, and Cu, the color of emission changes. These factors are known for their ability to change the wavelength of a blue color emission. According to O vacancy-associated transitions, PL(photoluminescence) spectra from Ga_2O_3 are commonly ruled using a large collection of transitions concentrated at about 399 nm at room temperature [43].

The majority of PL research does not any records in intrinsic emission inside the DUV(Deep Ultraviolet region) range (255nm–278 nm), but rather from the Ultraviolet (UV) range spectrum to the visible 350nm–600 nm. As a result, an ultraviolet-visible spectrometer is the best device used in determining the wavelength range based on the optical residences of all Ga_2O_3 polymorphs.
Because of the asymmetry in crystal morphologies, the optical residences of Ga_2O_3 also exhibit high-quality anisotropy [44]. Ga_2O_3 optical absorption occurs at distinct intensity transitions range Td coordinated Ga and O. Pleochroism in the vapor phase is an example of Ga_2O_3 optical residences. With the use of incident light, the light gets polarized in six unique angles, the response has led to the boom of Ga_2O_3 unmarried platelets. Ueda et al. [45] studied the optical features of single crystals developed by floating Zone (FZ), as illustrated in Fig. 4, to observe the spectrum of light from various angles. A slight absorption range of 4.90 - 4.59 eV may be seen in the angles of polarised light at E/b and E/c, respectively. E/b and E/c, interfered by threshold wavelengths of 253 nm and 270 nm, respectively.
When the angle between c and E was increased in optical transmission spectra, the wavelength spectrum was lowered.
optical features of natural Ga_2O_3 were still investigated using first-principles calculations based entirely on DFT in the generalized variation approximation used in Perdew–Burke–Ernzerhof method, Natural β-Ga_2O_3 is located between the Deep Ultraviolet (DUV)spectrum location (170–200 nm) with the best height absorption coefficient estimated as 2×10^5 cm^{-1} using the simulation model. Therefore, their transmittance is positioned in the Deep Ultraviolet(DUV) region at around 260 nm to 300 nm, with unique polarisation angles, Because of the optical absorption spectra in Fig. 5, which have the same wavelength location. As a result, every change is related to optical transmittance and absorption spectrum houses. Furthermore, based on our previous DFT work [46], Ga_2O_3 exhibits a DUV position in its height emission range of 100 nanometer to 280 nanometer .
Fabric synthesis, flaws, and doping can all be used to advance the optical characteristics of β-Ga_2O_3. The optical transmittance of Ga_2O_3 will rise when annealing time is extended [47]. By utilizing the low awareness of unfastened electrons within the dopants, Czochralski's approach gives excellent optical transmittance of Ga_2O_3 crystals [48].
The optical characteristics of Ga_2O_3 can also be obtained via the epitaxial approach, particularly within the metastable portion of β-Ga_2O_3. In the 4.9–5.6 eV range, the optical bandgap of α-Ga_2O_3 is marginally greater than that of β-Ga_2O_3 [51]. On the conduction band minimum, the band shape of α-Ga_2O_3 is similar to that of β-Ga_2O_3 is a very dispersive Ga 4s orbital nation (CBM). The valence band is well-known for having the same flatness as β-Ga_2O_3, which is found on the O 2p orbital nation. implies that β-Ga_2O_3 has a 5.39 eV oblique bandgap electricity.
Only a few investigations have been proposed into the optical homes of β- Ga_2O_3 and ϒ- Ga_2O_3 crystal systems. According to a recent study on the optical features of band gap for theβ - Ga_2O_3 crystal form, the valence band minimum is known for comparable flatness and a significant dispersion relation CBM. [52]. The computed optical bandgap is roughly 4.26 eV, according to Heyd–Scuseria–Ernzerh of relevant theory. The optical direct and oblique bandgaps of ϒ- Ga_2O_3 the crystal form are 5.30 eV and 5.15 eV [49].
The determination of a positive hue of the mild emission spectrum from various doped elements is a crucial component of Ga_2O_3optical properties. Every doping information of $Ga_2O_3$is listed in

Table *2* with the color and wavelength associated with it. With a transition metal, unusual earth, Ga_2O_3can display strong PL from wavelength emission. Eu^{3+}, Co, Cr, and Li all have a red color emission. Sn, Ce, and Tm, on the other hand, emit a yellow tint. Furthermore, Er, Ho, and Mn emit a green color.

Table 2 Emission spectrum of light with different doping elements.

Emission Light colour	Doping Element	Wavelength emission
Blue	Dy, Cu, Eu^{2+}	450-495 nm
Green	Er, Ho, Mn, Tb	495-570 nm
Red	Co, Li, Eu^{3+}	620-750 nm

Yellow	Sn, Tm, Ce	570-590 nm

Through $Eu^{2+}$and Dy-doped Ga_2O_3, a blue color emission is given. $Ga_2O_3$is enhanced by these doping elements in thin-film electroluminescence (TFEL) cells in digital display panels. As a result, inside the multicolor emissions of TFEL devices, high-depth luminescence can be obtained by using Ga_2O_3 with different doped values.

It has been given that monoclinic Ga_2O_3 in nanoflake form emits at 2.0 eV (red emission band) and 3.8 eV (blue emission band) (UV band). O and N vacancies, which are connected to the donor as well as acceptor levels in the establishment are responsible for the emission on the red band.

The source of the 3.8 eV emission, on the other hand, is yet unknown. Different emission peaks must be seen in the UV (3.3 eV), green, and blue areas of Ga_2O_3 layers produced using sapphire substrates employing HVPE [50]. The emission peak of the blue emission band was between 2.8 and 3.0 eV, while the green band at 2.4 eV.

transition between donors and acceptors given by the Oxygen(O) and Gallium (Ga) vacancies is shown by the green and blue peaks, respectively.. The intrinsic conductivity of Ga_2O_3 is n-type, which is ascribed to the recombination process [51]. Near the fascia's emission, which compensates for the deep levels [52]. Figure 6 shows the temperature-dependent cathodoluminescence of undoped Ga_2O_3 in the blue , green , and ultraviolet (UV) bands. The UV band's peak intensities fall as the temperature rises.

The temperature rise is almost unaffected. At 300K green and blue emissions predominate, allowing β-Ga_2O_3 to be manipulated usec for light-emitting optoelectronics appliances. The mechanism of the emission process is related to donor-acceptor pair (DAP) recombination [53]. The distance range between the donor atom and acceptor atom has a significant impact on the recombination timing of DAP emissions. The DAP band is comprises fluctuated energy associated with the Coulomb force contact between donors atom and acceptors atom during recombination. Because of the statistical fluctuation of the internal fields created by the density change of charged impurities, this substantial spatial fluctuation may cause further line broadening at the band's margins.

VIII. OPTOELECTRONIC APPLICATIONS OF Ga_2O_3 NANOSTRUCTURES

Ga_2O_3 nanostructures include nanowires, nanorods, nano blocks, and nanosheets, which are all low-dimensional crystalline Ga_2O_3 [54]. due to its compact size, high sensitivity, and quick response times. Additionally, adding dopants to Ga_2O_3 can improve its electrical and optical properties, increasing its performance efficiency.

Many methods for generating Ga_2O_3nanostructures have been examined, with the vapor-liquid-solid (VLS) technique being the most prevalent [55]. Supersaturated droplets are generated in this procedure, and metal alloys are used to dissolve the vapour component. During the development of the nanowires, the VLS process causes a solid phase to precipitate.

Using various types of catalysts, Ga_2O_3nanowires may produced on substrates by using the CVD process [64]. Au is employed as a catalyst to increase Ga_2O_3formations in nanowires, for example. The CVD process, like the hydrothermal method, is dependable and produces Ga_2O_3 structures of reasonably high quality. Ga2O3 nanostructures can be made through physical evaporation, laser ablation, organometallic CVD (MOCVD), and vapour phase epitaxy (VPE).

Apart from the VLS and CVD processes, there are other ways to generate high-quality Ga_2O_3nanostructures. Another well-known approach is the hydrothermal method, which was used by Ryou et al. [56] to make Ga_2O_3 Sn doped nanostructures. When compared to the pure structure of - Ga_2O_3, this approach resulted in a considerable increase in photocatalytic activities of Ga_2O_3 Sn doped under use of UV irradiation of 254 nm. Furthermore, Ga_2O_3nanostructures created uses the hydrothermal technique enable low-cost, simple, and easy-to-use nanostructure synthesis.

A field-effect transistor (MOSFET) construction with a thin layer of polycrystalline β-Ga_2O_3 back conductor for an optoelectronic device [57]. Sn dopants will replace the Gallium (Ga) atoms, allowing the device to more electrically capable a low current density of 21 mA/mm and exhibit power electronics cgaracterstics with treble exhibiting good light emission photoresponse at 254 nm, indicating the potential application for solar shade photodetectors. Meanwhile, Ga_2O_3has benefits over other typical broadband semiconductors in terms of optical features, such as very inexpensive ways of producing single-crystal structures and intrinsic sun blindness. Emissive display applications, such as TFELs, Schottky Barrier Diodes (SBDs), optoelectronic devices, such (LEDs) are examples of Ga_2O_3 -based devices.

The Ga_2O_3based solar-blind UV photodetector [58] is one of the most used optoelectronic applications. This gadget is commonly used in the military for missile early warning and UV communication. [23] Fire alarm and UV intensity sensing are some of the other applications [59].

The invention of a Ga_2O_3-based solar UV blind photodetector to help identify the presence of coronaviruses also has a lot of promise [59]. Recent improvements in solar cells are primarily focused on decreasing the effects of global warming and the greenhouse effect induced by continued fossil fuel use [60]. In terms of processing, the latest generation of solar cells is predicted to improve.

IX. SOLAR-BLIND UV PHOTODETECTORS

Ultraviolet (UV) photodetectors that are solar-blind are insensitive to infrared (IR) and closely UV radiation. However, sensible to UV wavelengths lower than 300 nm [61]. Solar-blind UV photodetector's primary function is to prevent visible light while transmitting Ultraviolet radiation by using different resources.

SBDs [62], photomultipliers [63], and photodiodes [64] represent current properties of solar-blind UV photodetectors. In the future, the solar-blind camera will be used to show power lines and identify electrical leakage in transmission cables. [65].

Suzuki et al. [66] presented the first solar-blind UV- Ga_2O_3 photodiodes. They have a semiconductive (100)-oriented β-Ga_2O_3 crystal structure, which they generated using the optical FZ approach. On the other side of the β-Ga_2O_3 crystal, Au–Schottky contact ,Ti/Al resistance unit contact are used. It entails hardening at 200^0C to improve the quality issue from 1.1 to 1.2 at 400^0C, as well as increasing the responsivity rate of the solar-blind actinic radiation photodiodes by magnitude up to 10^6 in the presence of 254 nm light. This strategy will boost the device photocurrent and reverse bias voltage.

The performance of β-Ga_2O_3based optoelectronic devices can be improved by fabricating an ultrawide bandgap Ga_2O_3employing grouping passivation [67]. As a result, for high-speed nanoelectronic devices, a low-dimensional structure of - Ga_2O_3 identical to the second with grouping passivation, may be obtained [68]. The same research also yielded useful information for developing better p-type Ga_2O_3optoelectronic devices. Furthermore, 2D-Ga_2O_3 structures will increase the absorption range of actinic radiation, expanding the optical spectrum's absorption range.

MBE was used by Guo et al. [69] to build a high-performance device with have vertical p–n heterojunction solar-blind photodetector. On a p-type (100) Si substrate, a (-201)-oriented - Ga_2O_3 was large, eventually generating p–n heterojunction solar-blind photodiodes. Conductors were made by depositing Ti/Al and Au on either side of the Ga_2O_3 layers. dark current magnitude of 8.5×107 A,photocurrent magnitude of 8× 10^4 A, the electrode operation is maximized in 254 nm lightweight condition and 3V reverse bias. At 254 nm, the photocurrent to dark current magnitude relationship was 9.4×10^2 A. At 365 nm, value was reduced to 6.2×10^2 A. Under ideal conditions of 254 nm and 3V reverse biasing voltage, maximum responsiveness can approach 370 A/W.

Liu et al. [70] employed the MBE approach to establish another manufacturing methodology for a photodetector with a solar blind. On an Al_2O_3 (0001) substrate, they imply a substantial (-201)-oriented -Ga_2O_3 layer. The resistance unit of this solar-blind UV photodetector valued 20 V biassing voltage. The dark and photocurrents are 0.04 and 438 nanoamperes, respectively. Within the spectral range of 210–280 nm, the photocurrent peak was 235 nm, which corresponds to the optimal range of light The maximum photoresponsivity was 259 A/W correspod 20 V, with rising and decay times of 0.02 seconds.

Using PLD to manufacture a high-quality Ga_2O_3thin film, an improved solar-blind photodetector was described [79]. Film thickness can change the surface roughness of the film, but it has no effect on grain size.. At the same bias voltage, the photocurrent was 16 A. Under the irradiation of a hydrogen atom lamp 4 millsecond and 104 millli secondScoreespond to rise time and decay timming, respectively.

He et al. [71] revealed a novel property when dual-band photodetector in combined β-Ga_2O_3 and black phosphorus heterojunction of p-n diode . MOCVD was used to generate the β-Ga_2O_3 layer heteroepitaxial on sapphire substrates, while mechanical exfoliation was used to deposit the BP layer. For the spectrum of IR and UV the made-up device had an honest spectral value of 88.5 mA W^{-1} and 1.24 mAW^{-1}, respectively. It illustrates the extraordinary potential of combining Ga_2O_3 with other superior materials to increase photodetector capabilities on the UV spectrum far side.

MSM solar-blind UV (Ultraviolet)photodetector [72] to build the Ga_2O_3 slim film on a glass substrate, several O pressure values is being used. The β-Ga_2O_3 thin film can then be employed to make a solar-blind UV photodetector's MSM structure. As the degree of O pressure rises, so does the responsiveness and response speed. At 50mTorr, this MSM UV photodetector corresponding high responsivity rate of 5 A/W. The detection value up to 10^{12} Jones to see the state of the incoming light is another novel feature of this MSM solar-blind photodetector. During the fabrication, Oxygen pressure should be carefully monitored to achieve the best results and construct a more advanced form of the sunlight transport for superior solar-blind photodetectors to be used.

The use of MgZnO UV photodetector obtained using RF thermionic valve sputtering was described by bird genus et al. [73]. At a voltage of -5 V biasing is applied, the low- maximum value of photo-dark current ratios were 5.93×10^{11}A and 5.69×10^4A concurrently. Due to the photoconduction effect, this device's external quantum potency was 63.3 %.However, this specific UV photodetector has a number of flaws that might cause dark current to flow out of the MgZnO MSM structure solar-blind UV

photodetector, affecting the responsivity magnitude ratio of UV to visible photon spectra. The characteristics of a - Ga_2O_3 solar-blind UV photodetector along with surface plasmon polariton (SPP) produced an Au ultrathin film that was undisputed [74]. The SPP method was used to increase the device's physical phenomenon qualities. An improvement in photoresponse was seen irradiation of 254 nanometer and 532nanometer, resulted that the photoelectric features improved.

Mistreatment of the polymer-assisted deposition (PAD) technology resulted in a full-grown Ga_2O_3 layer on a c-plane sapphire . [75]. The Ga_2O_3solar-blind UV photodetectors manufactured using this method have a smaller dark current and a shorter reaction time than those made using other procedures, likely nonaggressive CVD, Molecular beam epitaxy and PLD. With an applied bias, its responsivity was 4.2×10^3 A/W. The voltage might be as high as 20 volts.

Table 3 contrast the performance of solar-blind UV that will be researched in the coming years. Varied types of Ga_2O_3 based heterojunction devices have different detectivity, UV rejection magnitude relation, rising time, decay time, dark current, and photocurrent to dark current ratio (Iphoto/Idark).. The expansion and fabrication procedures of heterojunction devices are two different elements that will have an impact on the aforementioned characteristics.

Table 3 Comparison of performance of β-Ga_2O_3 UV photodetector with Growth method.

Types of Heterostructures	Detectivity(jones)	Rise time (s)	Decay time (s)	Spectral responsivity (AW^{-1})	I_{light}/I_{dark} Ratio	Method of Growth
β-Ga_2O_3 thin films	1.22×10^{15}	-	5.0×10^{-11}	190.08	$>10^3$	CVD
β- Ga_2O_3 thin films	-	0.32×10^{-6}	1.42×10^{-4}	0.102	6.04×10^4	PLD
β- Ga_2O_3 thin films	-	0.286	0.05	4.2×10^{-3}	-	PAD
β- Ga_2O_3 thin films	4.8×10^{11}	-	-	0.72	$>10^4$	Thermal-assisted conversion
ε- Ga_2O_3 thin films	1.2×10^{15}	-	0.024	230	-	MOCVD
ZnO/ Ga_2O_3	6.29×10^{12}	10^{-4}	9×10^{-4}	9.7×10^{-3}	-	CVD

X. LEDS

Ga_2O_3 is the most extensively used for manufacturing of LEDs due to Deep ultraviolet (DUV) spectrum region and n-type semiconductor characteristics. The LEDs were driven using a variety of nitride substrates, including GaN, InGaN, and AlGaN. The Ga_2O_3 crystalz and nitride substrate has a smaller offset than sapphire substrates, resulting in reduced stress and flaws at the interface. TCO electrodes were used in AlGaN-based UV LEDs The ITO Ga_2O_3, and Ag in a TCO electrode combine to produce an ITO/ Ga_2O_3/Ag/Ga_2O_3 multilayer, familiar to the MSM structure. LEDs are also covered by MSM. MSM layer has specific resistance value of 2.36×10^{-3} cm^2 and bandgap energy 5.11 eV, gves 92.8% transmission correspond to 365 nm wavength . The MSM structure sheet resistance. Is refduced by making Ag diffusioin layer. o AlGaN-based LEDs improved their electrical and optical parameters as a result of the suggested research.

Lee et al. [76] developed pin-transparent DUV LEDs using an active-emitting i- Ga_2O_3 thin film.. This is the first study to look into the possibility of Ga_2O_3-based metal oxide leads. LED structure made by InGaN was designed with a low-efficiency approach is used to stop non radiative process of combination at higher density [77]. The construction of vertical InGaN/GaN (MQW) multi-quantum well LEDs (VLEDs) on a Ga_2O_3substrate was developed for further research on this droop suppression application [78]. VLED has good optical efficiency, and the decreased effect aids in uniform heat distribution, decreasing the device's self-heating effect [79]. LEDs' total operating efficiency has been enhanced, and their possible uses have been expanded to include UV, yellow-green, blue, and infrared LEDs. Complex processing techniques, such as lift-and-transfer structures [80] vertical LEDs based on, are not required for fabricating devices employing this technology. AlGaN grown on Ga_2O_3 substrate has shown outstanding vertical stability.

With a peak quantum efficiency of more than 78% AlGaN grown on -βGa_2O_3 substrate has shown good vertical injection and emission of n-side. Due to the increasing possibility of radiative recombination pathways, quantum efficiency I,proved with injection current.GaN/AlGaN MQW structures built on an orientated Ga_2O_3 (- 201) substrate have been described [81]. When

contrast in sapphire substrate, the reduced density of dislocation defects achieved on - Ga2O3 led in better structural and optical capabilities..

In comparison to the planar LED, the nanorodrich LED has a tiny offset from the maximum position in the PL measurement. It also outperforms other planar and traditional LEDs in terms of light intensity.

The Ga_2O_3 layer's flaw elimination and transparency enhancement are the mechanisms behind this construction. However, further researches needed to increase the SNR of LEDs, which will improve overall stability and efficiency. Density dislocation and leakage current, which are smaller in modelled LEDs than in planar LED systems, are another illustration of the differences between modelled and planar geometries. [82]. The modeled LED quantum efficiency is also higher than that of planar arrangements.

When modeled LEDs were compared to planar LEDs, non-radiative recombination caused by high vector density becomes forward at a lower vector density. The sapphire substrate model for growing thin Ga_2O_3films can lower the energy barrier in LEDs, allowing more current to pass [83].

Zhou et al. revealed that Ga_2O_3 [84] based AlGaN UV LEDs with a specific resistance at contact about 2.36×10^3 cm^2 may achieve up to 93 % transmission at 365 nm. The bandgap energy cporesspond to 5.11 eV is achieved by Ag diffusion in the ITO/ Ga_2O_3 multilayer. As a result, doping of Ag element AlGaN-based LEDs reduces their optical properties. In Ga_2O_3 LEDs, rare earth metals like Erbium Er can be used as a doping [85]. green-yellowish emission spectrumlies between 520nm-600nm . Furthermore, the Electroluminescence(EL) measurement exhibits emission peaks that are comparable to those observed in the photoluminescence measurement. This discovery demonstrates that the device is capable. When electrically pumped, they emit at visible wavelengths, and so have a lot of depth in high-powered LED applications.

Rare earth elements, like Lutiteium and Europium , were used to fabricate Ga_2O_3-based LEDs in one work [86]. In range of 300 nm to 800 nm corresspond to visible lght range achieve optical transmittance was 83 %. These rare earth LEDs have bandgap energy of 3.96 eV, indicating that they can absorb a lot of light. Another benefit is the lack of interface cracks.

Another well-known application of the MSM semiconductor structure is in the manufacturing of solar cells. The MSM semiconductor heterostructure mechanism is used in solar cell design [87] to reduce the electric field's internal resistance and, as a result, increase electrical conductivity. The use of thin oxide buffers with the Cu2O absorber layer, such as β-Ga_2O_3 has decreased the conduction band offset difficulties . Inadequate efficiency is typically connected with [88]. Rizi et al. [89] created a model of a Cu_2O heterojunction solar cell with β-Ga_2O_3 used as active material.

XI. CONCLUSION AND FUTURE SCOPE

Several substantial problems face the field of Ga_2O_3based optoelectronic devices research. Decrease inn thermal conductivities and anisotropy in crystal structure, as well as electrical, and optical character of Ga_2O_3, are among these concerns. The doping method can be used to solve almost any problem. Doping elements such as Magneses(Mg), Arsenic, Nitrogen (N) can be included radically alter Ga_2O_3 intrinsic characteristics [90]. P-type doping, for example, allows for shallow acceptor and hole processes. The Ga_2O_3 structure allows for conduction. With a p-type dopingin element, this process will make Ga_2O_3 electrically insulated. As a result, the future focus of β-Ga_2O_3 based optoelectronic device development is expected to be on p-type doping improvement. Adjusting the orientation to optimized surface energy [91] is another solution to Ga_2O_3 anisotropic characteristics. The substrates (010) and (001) have always been employed in the growing process. Changing the direction of Ga_2O_3 can have a big impact. Its anisotropic electrical conductivity and optical absorption efficiencies should be increased. The majority of research on this topic is still centered on determining the optimal Ga_2O_3 orientation to maximize device efficiency Additionally, this treatment can aid in improving performance.indium oxide (In_2O_3) and Al_2O_3 are examples of other III–V materials. What has been Ga_2O_3 most compelling feature? Ga_2O_3 has high thermal improved breakdown voltage, and ultrawide bandgap (UWB) energy also improved , according to present researches. Ga_2O_3 has an outstanding FOM for high power device and large speed applications due to its physical characteristics. Bulk Ga_2O_3 substrates, on the other hand, may be mass-produced and made easilyand availe at a reasonable cost. Assisting in the production of more homoepitaxial Ga_2O_3 devices Ga_2O_3 substrates are simple to use in optoelectronic device applications.To generate $(AlGa)_2O_3$ or $(InGa)_2O_3$ heterostructures, combine with additional metals such as Al and In. These substances are very common. High-performance optoelectronic devices are made from a variety of materials. Ga_2O_3 is used in the production of high-performance solar cells and LEDs also has a lot of promise. Additional study and effort are being put towards achieving goals, including the use of Ga_2O_3 as buffer for solar cells. layer [92] and Ga_2O_3 and organic materials hybrid methods [93]. Ga_2O_3 is used in optoelectronics for a variety of reasons. The goal of technology like LEDs , solar cells are used to reduce electrical consumption and so advance towards further substainable development.

XII. SUMMARY

The characteristics of Ga_2O_3 and their applications in optoelectronic devices application were the focus of this review. Polymorphism, material characteristics, optical properties of Ga_2O_3 are all covered. Ga_2O_3 thin-film applications are also reviewed, with a focus on sun-blind photodetectors,solar cells and LEDs. The available of bulk substrate is a key benefit of β-Ga_2O_3.

The performance of semiconductor devices is determined by a number of factors. Because β-Ga_2O_3 is particularly sensitive to detecting dislocation density, it is used to study its crystal structure. However, some difficulties, such as limited access, must be inscribed . To increase the characterisitics of Ga_2O_3-based devices, thermal conductivity and value of phonon scattering must be included .

It is developed during the last few decades as a material that tolerate high temperature range, perform well in power electronics device applications, and exhibit strong breakdown -electric- strength of greater than 1 (keV) [94], and it is also useful in solar-blind -Ultra violet (UV) light prediction [95].therfore results there are still some concerns about using Ga_2O_3 as a semiconductor device material. Thermal management in power electrical devices is one of the most serious issues with Ga_2O_3. The use of Ga_2O_3 in the development. The topic of optoelectronic devices has been fully addressed. The majority of solar-blind UV(Ultra violet) photodetectors are made up with heteroepitaxial materials β-Ga_2O_3. planar configuration with various materials,metal-semiconductor, p–n junction electrode geometries is used to make optoelectronic devices .

LEDs having β-Ga_2O_3 wmission in Deep ultraviolet region(DUV) up to the range of visible spectrum is recorded by various researchers . When GaN based LED is epitaxially grown , they can be used as a buffer layer. Because Ga_2O_3 and GaN exhibit same lattice constant numeriacal values, the problem related to strain at the contact is eliminated or reduced. VLEDs have a lot of potential because of their high output power and decreasein input power. The advancement of solar cell using Ga_2O_3 is fascinating topic . The present state of solar cell research and performance were discussed, with a focus on using Ga_2O_3 as a passivation layer. Despite the extensive evaluations and tremendous progressive increase made in Ga_2O_3, much work remains to be done in order to achieve a mature and optimized technologies . Doping, for example, is a problem. To fully realize the potential of Ga_2O_3, particularly in the optoelectronic industry, research and fabrication methodologies should be made. The current state of research in the investigation of β-Ga_2O_3 as a prospective contender for diverse applications is summarised in this publication. Recent advances have been made in bulk and thin-film growth, defect and impurity control, and other areas. Furthermore, it is critical to comprehend the impact of different growth factors on the optical, electrical characterization of β-Ga_2O_3 . Fabrication for good quality Ga_2O_3 thin films is a topic that should be investigated more in the future.

XIII. ACKNOWLEDGMENT

This work is done by the author and thankful to my supervisor and Institute of Engineering and Technology, Lucknow for supporting to done my work .

REFERENCES

[1] K. Sasaki, M. Higashiwaki, A. Kuramata, T. Masui, S. Yamakoshi, Journal of Crystal Growth 378 (2013) 591–595.
[2] S.J. Pearton, J. Yang, P.H. Cary, F. Ren, J. Kim, M.J. Tadjer, M.A. Mastro, Applied Physics Reviews 5 (2018) 011301.
[3] D. Zhang, S. Dong, Progress in Natural Science: Materials International 29 (2019) 277–284.
[4] J. Zhang, J. Shi, D.C. Qi, L. Chen, K.H.L. Zhang, APL Materials 8 (2020) 020906.
[5] L. Li, W. Wei, M. Behrens, Solid State Sciences 14 (2012) 971–981.
[6] (n.d.).
[7] Z. Guo, A. Verma, X. Wu, F. Sun, A. Hickman, T. Masui, A. Kuramata, M. Higashiwaki, D. Jena, T. Luo, Applied Physics Letters 106 (2015) 111909.
[8] Z. Galazka, R. Uecker, D. Klimm, K. Irmscher, M. Naumann, M. Pietsch, A. Kwasniewski, R. Bertram, S. Ganschow, M. Bickermann, ECS Journal of Solid State Science and Technology 6 (2017) Q3007–Q3011.
[9] E.G. Víllora, K. Shimamura, T. Ujiie, K. Aoki, Applied Physics Letters 92 (2008) 202118.
[10] Y. Tomm, J.M. Ko, A. Yoshikawa, T. Fukuda, Solar Energy Materials and Solar Cells 66 (2001) 369–374.
[11] K. Irmscher, M. Naumann, M. Pietsch, Z. Galazka, R. Uecker, T. Schulz, R. Schewski, M. Albrecht, R. Fornari, Physica Status Solidi (a) 211 (2014) 54–58.
[12] Z. Galazka, R. Uecker, D. Klimm, K. Irmscher, M. Naumann, M. Pietsch, A. Kwasniewski, R. Bertram, S. Ganschow, M. Bickermann, ECS Journal of Solid State Science and Technology 6 (2017) Q3007–Q3011.
[13] M. Higashiwaki, K. Sasaki, A. Kuramata, T. Masui, S. Yamakoshi, Physica Status Solidi (a) 211 (2014).
[14] T. Harwig, F. Kellendonk, Journal of Solid State Chemistry 24 (1978) 255–263.
[15] M. Slomski, N. Blumenschein, P.P. Paskov, J.F. Muth, T. Paskova, Journal of Applied Physics 121 (2017) 235104.
[16] M. Higashiwaki, K. Sasaki, A. Kuramata, T. Masui, S. Yamakoshi, Physica Status Solidi (a) 211 (2014).
[17] Wagner, M. Baldini, D. Gogova, M. Schmidbauer, R. Schewski, M. Albrecht, Z. Galazka, D. Klimm, R. Fornari, Physica Status Solidi (a) 211 (2014) 27–33.
[18] Murakami, K. Nomura, K. Goto, K. Sasaki, K. Kawara, Q. Tu Thieu, R. Togashi, Y. Kumagai, M. Higashiwaki, A. Kuramata, S. Yamakoshi, B. Monemar, A. Koukitu, Applied Physics Express 8 (2015) 015503.

[19] S. Rafique, L. Han, H. Zhao, Physica Status Solidi (a) 214 (2017) 1700063.
[20] E.G. Víllora, K. Shimamura, K. Kitamura, K. Aoki, Applied Physics Letters 88 (2006) 031105.
[21] K. Sasaki, A. Kuramata, T. Masui, E.G. Víllora, K. Shimamura, S. Yamakoshi, Applied Physics Express 5 (2012) 035502.
[22] M.H. Wong, K. Sasaki, A. Kuramata, S. Yamakoshi, M. Higashiwaki, Applied Physics Letters 106 (2015) 032105.
[23] K. Sasaki, A. Kuramata, T. Masui, E.G. Víllora, K. Shimamura, S. Yamakoshi, Applied Physics Express 5 (2012) 035502.
[24] E. Ahmadi, O.S. Koksaldi, S.W. Kaun, Y. Oshima, D.B. Short, U.K. Mishra, J.S. Speck, Applied Physics Express 10 (2017) 041102.
[25] M. Baldini, M. Albrecht, A. Fiedler, K. Irmscher, R. Schewski, G. Wagner, ECS Journal of Solid State Science and Technology 6 (2016) Q3040.
[26] X. Du, Z. Li, C. Luan, W. Wang, M. Wang, X. Feng, H. Xiao, J. Ma, Journal of Materials Science 50 (2015) 3252–3257.
[27] Murakami, K. Nomura, K. Goto, K. Sasaki, K. Kawara, Q. Tu Thieu, R. Togashi, Y. Kumagai, M. Higashiwaki, A. Kuramata, S. Yamakoshi, B. Monemar, A. Koukitu, Applied Physics Express 8 (2015) 015503.
[28] S. Rafique, M.R. Karim, J.M. Johnson, J. Hwang, H. Zhao, Applied Physics Letters 112 (2018) 052104.
[29] S. Rafique, L. Han, A.T. Neal, S. Mou, M.J. Tadjer, R.H. French, H. Zhao, Applied Physics Letters 109 (2016) 132103.
[30] M. Mohamed, C. Janowitz, I. Unger, R. Manzke, Z. Galazka, R. Uecker, R. Fornari, J.R. Weber, J.B. Varley, C.G. van de Walle, Applied Physics Letters 97 (2010) 211903
[31] M. Higashiwaki, K. Sasaki, A. Kuramata, T. Masui, S. Yamakoshi, Applied Physics Letters 100 (2012) 013504.
[32] S. Ahn, F. Ren, J. Kim, S. Oh, J. Kim, M.A. Mastro, S.J. Pearton, Applied Physics Letters 109 (2016) 062102.
[33] M. Nazarzadehmoafi, S. Machulik, F. Neske, V. Scherer, C. Janowitz, Z. Galazka, M. Mulazzi, R. Manzke, Applied Physics Letters 105 (2014) 162104.
[34] K. Konishi, K. Goto, H. Murakami, Y. Kumagai, A. Kuramata, S. Yamakoshi, M. Higashiwaki, Applied Physics Letters 110 (2017) 103506.
[35] Kim, C. Jin, S. An, C. Lee, Ceramics International 38 (2012) 3563–3567.
[36] H.F. Mohamed, C. Xia, Q. Sai, H. Cui, M. Pan, H. Qi, Journal of Semiconductors 40 (2019) 011801.
[37] M. Ueno, K.J. Kim, K. Kamada, T. Nihei, M. Yoshino, A. Yamaji, S. Toyoda, H. Sato, Y. Yokota, S. Kurosawa, Y. Ohashi, M. Nikl, V. Kochurikhin, A. Yoshikawa, Journal of Crystal Growth 539 (2020) 125513.
[38] (n.d.).
[39] A.M. Hassanien, A.A. Atta, M.M. El-Nahass, S.I. Ahmed, A.A. Shaltout, A.M. Al-Baradi, A. Alodhayb, A.M. Kamal, Optical and Quantum Electronics 52 (2020) 1–16.
[40] A.M. Hassanien, A.A. Atta, M.M. El-Nahass, S.I. Ahmed, A.A. Shaltout, A.M. Al-Baradi, A. Alodhayb, A.M. Kamal, Optical and Quantum Electronics 52 (2020) 1–16.
[41] M.J. Tadjer, J.L. Lyons, N. Nepal, J.A. Freitas, A.D. Koehler, G.M. Foster, ECS Journal of Solid State Science and Technology 8 (2019) Q3187.
[42] T. Harwig, F. Kellendonk, S. Slappendel, Journal of Physics and Chemistry of Solids 39 (1978) 675–680.
[43] (n.d.).
[44] J. bin Cho, G. Jung, K. Kim, J. Kim, S.K. Hong, J.H. Song, J.I. Jang, Journal of Physical Chemistry C 125 (2021) 1432–1440.
[45] N. Ueda, H. Hosono, R. Waseda, H. Kawazoe, Applied Physics Letters 71 (1998) 933.
[46] A.K. Mondal, M.A. Mohamed, L.K. Ping, M.F.M. Taib, M.H. Samat, M.A.S.M. Haniff, R. Bahru, Materials 2021, Vol. 14, Page 604 14 (2021) 604.
[47] Y. Yao, S. Okur, L.A.M. Lyle, G.S. Tompa, T. Salagaj, N. Sbrockey, R.F. Davis, L.M. Porter, Http://Mc.Manuscriptcentral.Com/Tmrl 6 (2018) 268–275.
[48] Z. Galazka, R. Uecker, D. Klimm, K. Irmscher, M. Naumann, M. Pietsch, A. Kwasniewski, R. Bertram, S. Ganschow, M. Bickermann, ECS Journal of Solid State Science and Technology 6 (2017) Q3007–Q3011.
[49] M. Pavesi, F. Fabbri, F. Boschi, G. Piacentini, A. Baraldi, M. Bosi, E. Gombia, A. Parisini, R. Fornari, Materials Chemistry and Physics 205 (2018) 502–507.
[50] G. Pozina, C.W. Hsu, N. Abrikossova, M.A. Kaliteevski, C. Hemmingsson, Scientific Reports 2020 10:1 10 (2020) 1–9.
[51] A. Singh, O. Koksal, N. Tanen, J. McCandless, D. Jena, H. Xing (Grace), H. Peelaers, F. Rana, Applied Physics Letters 117 (2020) 072103.
[52] R.K. Mondal, S. Adhikari, V. Chatterjee, S. Pal, Materials Research Bulletin 140 (2021) 111258.
[53] B. Fu, G. He, W. Mu, Y. Li, B. Feng, K. Zhang, H. Wang, J. Zhang, S. Zhang, Z. Jia, Y. Shi, Y. Li, S. Ding, X. Tao, CrystEngComm 23 (2021) 3724–3730.
[54] C.C. Wang, B.C. Lee, F.S. Shieu, H.C. Shih, Chemical Physics Letters 753 (2020) 137624.
[55] S. Kumar, G. Sarau, C. Tessarek, M.Y. Bashouti, A. Hähnel, S. Christiansen, R. Singh, Journal of Physics D: Applied Physics 47 (2014) 435101.
[56] H. Ryou, T.H. Yoo, Y. Yoon, I.G. Lee, M. Shin, J. Cho, B.J. Cho, W.S. Hwang, ECS Journal of Solid State Science and Technology 9 (2020) 045009.
[57] Y. Yoon, S. Kim, I.G. Lee, B.J. Cho, W.S. Hwang, Materials Science in Semiconductor Processing 121 (2021) 105430.
[58] D. Guo, Q. Guo, Z. Chen, Z. Wu, P. Li, W. Tang, Materials Today Physics 11 (2019) 100157.
[59] F. Ren, J. Ye, S. Gu, X. Chen, Photonics Research, Vol. 7, Issue 4, Pp. 381-415 7 (2019) 381–415.
[60] M.K. Assadi, S. Bakhoda, R. Saidur, H. Hanaei, Renewable and Sustainable Energy Reviews 81 (2018) 2812–2822.
[61] J. Xu, W. Zheng, F. Huang, Journal of Materials Chemistry C 7 (2019) 8753–8770.
[62] M. Xiao, Y. Ma, K. Cheng, K. Liu, A. Xie, E. Beam, Y. Cao, Y. Zhang, IEEE Electron Device Letters 41 (2020) 1177–1180.
[63] Y.H. An, D.Y. Guo, S.Y. Li, Z.P. Wu, Y.Q. Huang, P.G. Li, L.H. Li, W.H. Tang, Journal of Physics D: Applied Physics 49 (2016) 285111.
[64] A. Atilgan, A. Yildiz, U. Harmanci, M.T. Gulluoglu, K. Salimi, Materials Today Communications 24 (2020) 101105.
[65] K. Kojima, Y. Yoshida, M. Shiraiwa, Y. Awaji, A. Kanno, N. Yamamoto, A. Hirano, Y. Nagasawa, M. Ippommatsu, S.F. Chichibu, Applied Physics Letters 117 (2020) 031103.
[66] R. Suzuki, S. Nakagomi, Y. Kokubun, N. Arai, S. Ohira, Applied Physics Letters 94 (2009) 222102.
[67] K. Ghosh, U. Singisetti, Journal of Applied Physics 122 (2017) 035702.
[68] L. Dong, S. Zhou, L. Gong, W. Wang, L. Zhang, C. Yang, J. Yu, W. Liu, Journal of Materials Chemistry C 8 (2020) 12551–12559.
[69] X.C. Guo, N.H. Hao, D.Y. Guo, Z.P. Wu, Y.H. An, X.L. Chu, L.H. Li, P.G. Li, M. Lei, W.H. Tang, Journal of Alloys and Compounds 660 (2016) 136–140.
[70] X.Z. Liu, P. Guo, T. Sheng, L.X. Qian, W.L. Zhang, Y.R. Li, Opt Mater (Amst) 51 (2016) 203–207.
[71] T. He, C. Li, X. Zhang, Y. Ma, X. Cao, X. Shi, C. Sun, J. Li, L. Song, C. Zeng, K. Zhang, X. Zhang, B. Zhang, Physica Status Solidi (a) 217 (2020) 1900861.
[72] X.Z. Liu, P. Guo, T. Sheng, L.X. Qian, W.L. Zhang, Y.R. Li, Opt Mater (Amst) 51 (2016) 203–207.
[73] X. Chen, W. Mi, J. Wu, Z. Yang, K. Zhang, J. Zhao, C. Luan, Y.L. Wei, Vacuum 180 (2020) 109632.

[74] Y. An, X. Chu, Y. Huang, Y. Zhi, D. Guo, P. Li, Z. Wu, W. Tang, Progress in Natural Science: Materials International 26 (2016) 65–68.
[75] X. Dai, Q. Zheng, X. Zhang, Y. Wang, H. Ren, G. Xiang, Materials Letters 284 (2021) 128912.
[76] H.Y. Lee, C.H. Lin, C.T. Lee, IEEE Photonics Technology Letters 32 (2020) 941–943.
[77] Y.S. Yoo, J.H. Na, S.J. Son, Y.H. Cho, Scientific Reports 2016 6:1 6 (2016) 1–9.
[78] M.M. Muhammed, N. Alwadai, S. Lopatin, A. Kuramata, I.S. Roqan, ACS Applied Materials and Interfaces 9 (2017) 34057–34063.
[79] W. Li, X. Zhang, R. Meng, J. Yan, J. Wang, J. Li, T. Wei, Micromachines 2019, Vol. 10, Page 322 10 (2019) 322.
[80] X. Chen, W. Mi, J. Wu, Z. Yang, K. Zhang, J. Zhao, C. Luan, Y.L. Wei, Vacuum 180 (2020) 109632.
[81] X. Dai, Q. Zheng, X. Zhang, Y. Wang, H. Ren, G. Xiang, Materials Letters 284 (2021) 128912
[82] Y.S. Yoo, J.H. Na, S.J. Son, Y.H. Cho, Journal of Physics D: Applied Physics 49 (2016) 095101.
[83] A. v. Almaev, V.I. Nikolaev, S.I. Stepanov, A.I. Pechnikov, A. v. Chikiryaka, N.N. Yakovlev, V.M. Kalygina, V. v. Kopyev, E. v. Chernikov, Journal of Physics D:
[84] S. Liang, Q. Zhou, X. Li, M. Zhong, H. Wang, Nanomaterials 2019, Vol. 9, Page 403 9 (2019) 403.
[85] Z. Chen, G. Subhash, J.S. Tulenko, Journal of Nuclear Materials 475 (2016) 1–5.
[86] S. Kunuku, Y.-C. Chen, C.-J. Yeh, al -, K. Ohdaira, T. Fujiwara, Y. Endo, IOP Conference Series: Materials Science and Engineering 872 (2020) 012062.
[87] Y. Lv, S. Duan, R. Wang, Progress in Natural Science: Materials International 30 (2020) 1–12.
[88] H.Y. Lee, C.H. Lin, C.T. Lee, IEEE Photonics Technology Letters 32 (2020) 941–943.
[89] M. Toghyani Rizi, M.H. Shahrokh Abadi, M. Ghaneii, Optik (Stuttg) 155 (2018) 121–132.
[90] M. Higashiwaki, A. Kuramata, H. Murakami, Y. Kumagai, Journal of Physics D: Applied Physics 50 (2017) 333002.
[91] Y. Hinuma, T. Kamachi, N. Hamamoto, M. Takao, T. Toyao, K.I. Shimizu, Journal of Physical Chemistry C 124 (2020) 10509–10522.
[92] K.O. Hara, C.T. Trinh, K. Arimoto, J. Yamanaka, K. Nakagawa, Y. Kurokawa, T. Suemasu, N. Usami, 2017 IEEE 44th Photovoltaic Specialist Conference, PVSC 2017 (2017) 2209–2212.
[93] M. García-Carrión, J. Ramírez-Castellanos, E. Nogales, B. Méndez, C.C. You, S. Karazhanov, E.S. Marstein, Materials Letters 261 (2020) 127088.
[94] H. Shen, K. Baskaran, Y. Yin, K. Tian, L. Duan, X. Zhao, A. Tiwari, Journal of Alloys and Compounds 822 (2020) 153419.
[95] T. He, C. Li, X. Zhang, Y. Ma, X. Cao, X. Shi, C. Sun, J. Li, L. Song, C. Zeng, K. Zhang, X. Zhang, B. Zhang, Physica Status Solidi (a) 217 (2020) 1900861.

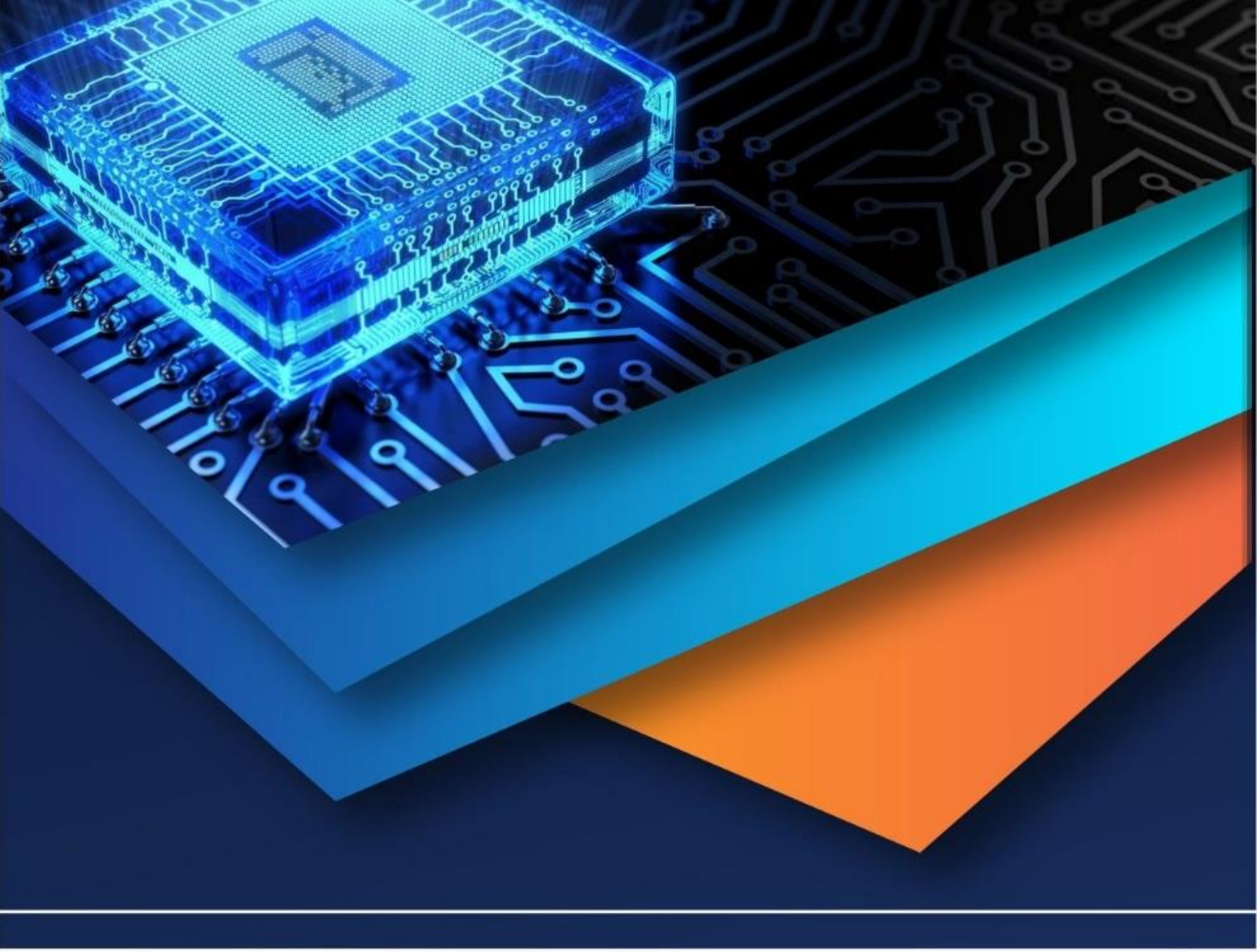

10.22214/IJRASET

45.98

IMPACT FACTOR: 7.129

IMPACT FACTOR: 7.429

INTERNATIONAL JOURNAL FOR RESEARCH

IN APPLIED SCIENCE & ENGINEERING TECHNOLOGY